Heat Mass Transfer (2017) 53:3545–3563
DOI 10.1007/s00231-017-2061-0

ORIGINAL

Experimental and numerical study on heat transfer enhancement of flat tube radiator using Al_2O_3 and CuO nanofluids

Sobin Alosious[1] · Sarath S R[2] · Anjan R Nair[2] · K Krishnakumar[2]

Received: 15 October 2016 / Accepted: 11 May 2017 / Published online: 17 June 2017
© Springer-Verlag Berlin Heidelberg 2017

Abstract Forced convective heat transfer of Al_2O_3 and CuO nanofluids through flat tube automobile radiator were studied experimentally and numerically. Nanofluids of 0.05% volume concentrations were prepared with Al_2O_3 and CuO nanoparticles having diameter below 50 *nm*. The working fluid recirculates through an automobile flat tube radiator with constant inlet temperature of 90 °C. Experiments were conducted by using water and nanofluids by varying the Reynolds numbers from 136 to 816. The flat tube of the radiator with same dimensions were modeled and numerically studied the heat transfer. The model includes the thickness of tube wall and also considers the effect of fins in the radiator. Numerical studies were carried out for six different volume concentrations from 0.05% to 1% and Reynolds number varied between 136 and 816 for both nanofluids. The results show an enhancement in heat transfer coefficient and effectiveness of radiator with increase in Reynolds number and volume concentration. A maximum enhancement of 13.2% and 16.4% in inside heat transfer coefficient were obtained for 1% concentration of CuO and Al_2O_3 nanofluids respectively. However increasing the volume concentration causes an increase in viscosity and density, which leads to an increase in pumping power. For same heat rejection of water, the area of the radiator can be reduced by 2.1% and 2.9% by using 1% concentration of CuO and Al_2O_3 nanofluids respectively. The optimum values of volume concentration were found to be 0.4% to 0.8% in which heat transfer enhancement dominates pumping power increase. Al_2O_3 nanofluids gives the maximum heat transfer enhancement and stability compared to CuO nanofluids.

Keywords Nanofluids · Al_2O_3 · CuO · Radiator · Flat tube · Heat transfer · Nusselt number · Colburn-Chilton factor

Nomenclature

$\dot{m}$	Mass flow rate, kg/s
A	Area, m^2
C_f	Friction factor
C_p	Specific heat capacity, J/kgK
d	Diameter, m
h	Heat transfer coefficient, W/m^2K
j	Colburn-Chilton factor
k	Thermal conductivity, W/mK
L	Length, m
NTU	Number of transfer units
Nu	Nusselt number
P	Pressure, N/m^2
Q	Heat transfer rate, W
Re	Reynolds number
T	Temperature, K
T_0	Reference temperature, 273 K
U	Overall heat transfer coefficient, W/m^2K
V	Velocity, m/s
W	Pumping power, W
w	Weight, N

✉ Anjan R Nair
anjanrn@gmail.com

[1] Department of Mechanical Engineering, Holy Kings College of Engineering and Technology, Pampakuda, India

[2] Department of Mechanical Engineering, College of Engineering Trivandrum, Triruvananthapuram, India

Greek Symbols

κ	Boltzmann constant, 1.381 $\times 10^{-23}$ J/K
μ	Viscosity, Ns/m^2
ϕ	Volume concentration, %
ρ	Density, kg/m^3
ε	Effectiveness
φ	Volume fraction

Subscripts

a	Air
avg	Average
bf	Base fluid
hyd	Hydraulic diameter
in	Inlet
nf	Nanofluid
np	Nanoparticle
out	Outlet
t	Tube

1 Introduction

Performance of automobile engines can be improved by effective removal of heat from the engine. There are different heat transfer enhancement techniques used to increase the heat removal such as increasing surface area, efficient geometry, increase in coolant flow rate, improving the properties of heat transfer fluid etc. Introduction of flat tube radiators into automobile causes an improvement in heat transfer. Flat tube radiators are widely used due their higher heat transfer area and lower air side pressure drop compared to round tube radiators of the same capacity. Improving the properties of heat transfer fluids can considerably enhance the heat transfer. Development of nanofluids opens further possibilities in increasing heat transfer. Conventional heat transfer fluids such as water, engine oil, ethylene glycol, refrigerants etc. have very poor heat transfer performances. These conventional fluids can be replaced by nanofluids. Nanofluids are colloidal suspensions of nanometer sized particles called nanoparticles such as metal oxide, carbon nano-tubes or graphene.

Many experimental works were conducted for the preparation of nanofluids and one step method and two step method were suggested to be feasible [1–7]. Studies were carried out to find the mechanism of variation in thermal properties when nanoparticles were added in the base fluid [8, 9]. The authors reported an enhancement in heat transfer properties compared to conventional heat transfer fluids with the addition of nanoparticles. The enhancement in heat transfer properties were due to the considerable improvement in thermal conductivity. The thermal conductivity of nanofluid increases due to addition of higher thermal conductivity nanoparticles and due to Brownian motion of nanoparticles in the base fluid [10]. Bigdeli et al. [11] reviewed the heat and mass transfer phenomena in nanofluid coolants with special focus on automotive applications. The study presents several theoretical and empirical models describing nanofluid thermal conductivity, viscosity, specific heat capacity and density. They also highlighted the advantages of nanofluids as coolant for automobile radiators and suggested guidelines for the design and usage. Kakaç and Pramuanjaroenkij [12] reviewed the convective heat transfer enhancement by nanofluids for single phase and two phase treatments. The studies showed that the two-phase mixture model and single-phase model results are very similar due to the low velocities of the phases relative to each other. The Eulerian two-phase model is more complex and computationally expensive thus single phase method is desirable for nanofluid modeling. Krishnakumar et al. [13] numerically studied the enhancement in heat transfer and increase in pumping power of CuO-Water nanofluid in automotive diesel engine radiator. CuO-water nanofluid with 20 *nm* nanoparticle size for 0-2% volume concentration under turbulent flow conditions were tested. The results shows an enhancement of 10% in heat transfer coefficient and 23.8% increase in pumping power for 2% volume concentration and Reynolds number 6000. Chiam et al. [14] measured the thermal conductivity and viscosity of Al_2O_3 nanofluids for different based ratio of water and Ethylene glycol mixture. They found that The average thermal conductivity enhancement of Al_2O_3 nanofluids in the three base ratios varied from 2.6 to 12.8%. As the percentage of ethylene glycol increases, the nanofluids have more enhancement. The properties enhancement of the Al_2O_3 nanofluids depends on concentration, temperature, and based ratio. Bayat and Nikseresht [15] investigated different base fluid effects on the nanofluids heat transfer and pressure drop. The results indicate that the averaged heat transfer coefficient and wall shear stress increase with increasing parameters like, mass of ethylene glycol in the water base fluid, solid concentration and Reynolds number. Rashmi R et al. [16] studied the effect of convective heat transfer in an automobile radiator using hybrid nanofluids. For the same radiator size and heat transfer rate, coolant flow rate decreases by 3.1% and pumping power increases by 1.9% for Ag hybrid nanofluids as compared to base fluid, which leads to increase in engine thermal efficiency and hence reduction in engine fuel consumption.

Vajjha et al. [17] numerically studied the fluid dynamic and heat transfer performance of Al_2O_3 and CuO nanofluids in flat tube radiator. Simulation were carried out for six different concentrations and Reynolds number varying between 100 to 2000. The analysis shows an increase in heat transfer coefficient with increase in Reynolds number and concentration.The average skin friction coefficient increased 2.7 times that of the base fluid for 6% concentration of Al_2O_3. Peyghambarzadeh et al. [18, 19]

Table 1 Thermophysical properties of Al_2O_3 and CuO nanoparticles. [20]

Material	Al_2O_3	CuO
Diameter	$<50\ nm$	$<50\ nm$
Purity	99%	99%
Density	$3970\ kg/m^3$	$6510\ kg/m^3$
Specific heat capacity	$525\ J/kgK$	$540\ J/kgK$
Thermal conductivity	$17.65\ W/mK$	$33\ W/mK$

experimentally evaluated the cooling performance of automobile radiator with water and ethylene glycol based nanofluids. The experiments were conducted for five different concentrations in the range of 0.1% to 1% and flow rate varied between 2 to 6 *l/min*. The effect of inlet temperature was analysed by varying inlet temperature. A maximum of 45% enhancement in heat transfer coefficient and an increase of 40% in Nusselt number were obtained for 1% volume concentration.

The objective of the present study is to experimentally and numerically evaluate the heat transfer enhancement and hydrodynamic behavior of Al_2O_3-water and CuO-water nanofluid in an automobile flat tube radiator compared to conventional coolants. The experiments were carried out for different Reynolds numbers and volume concentrations of nanofluid. Numerical modeling and computation of the same flat tube radiator were done. The numerical simulations which were validated with the experimental method can give flexibility in wide range of operating parameters. The variation of Nusselt number, friction factor, effectiveness of radiator, Colburn-Chilton factor etc. with Reynolds number were obtained. Thus optimum working condition such as volume concentration of nanofluid and mass flow rate of coolant were obtained by conducting experiments and numerical simulations.

2 Experimental method

Nanofluids of 0.05% volume concentrations were prepared with Al_2O_3 and CuO nanoparticles having diameter below 50 *nm*. The working fluid recirculates through an automobile flat tube radiator with constant inlet temperature of 90 °C. Experiments were conducted by using water and nanofluids by varying the Reynolds numbers from 136 to 816.

2.1 Preparation of nanofluid

Two-step method is the most widely used method for the preparation of nanofluids. Nanoparticles, nanofibers, nanotubes, or other nanomaterials used in this method are first produced as dry powders by chemical or physical methods. Then, the nanosized powder will be dispersed into a fluid in the second processing step with the help of intensive magnetic force agitation, ultrasonic agitation, high-shear mixing, homogenizing, or ball milling. Al_2O_3 and CuO nanoparticles were purchased from Sigma Aldrich Chemicals Bangalore. The thermophysical properties of Al_2O_3 and CuO nanoparticles are shown in Table 1. Nanofluids of 0.05% volume concentrations were prepared by dispersing Al_2O_3 and CuO nanoparticles in de-ionized water by using probe type sonicator. Surfactants were added to avoid sedimentation of nanoparticles in the base fluid. Sodium dodecyl benzene sulphate (SDBS) surfactant with 1/4th weight of nanoparticles were added. Samples of the prepared nanofluids are shown in Fig. 1. Volume concentration of nanofluid is calculated by using the following (1).

$$\phi = \left[\frac{(w_{np}/\rho_{np})}{(w_{np}/\rho_{np}) + (w_{bf}/\rho_{bf})}\right] \times 100 \tag{1}$$

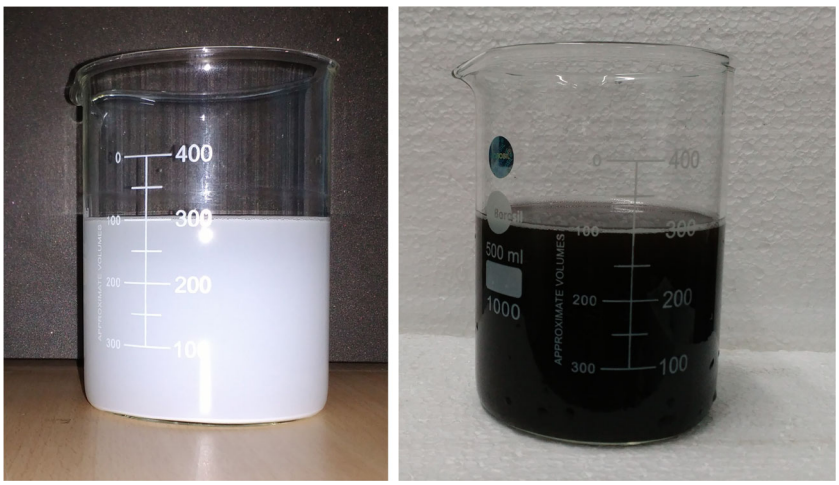


Fig. 1 Al_2O_3-water and CuO-water nanofluid (0.05%)

2.2 Nanofluid physical properties

The thermophysical properties of nanofluids such as density, specific heat capacity, thermal conductivity and viscosity can be evaluated by the following (2–7). These properties depends on properties of nanoparticle, concentration of nanoparticle and properties of the base fluid.

2.2.1 Specific heat capacity and density

The equations for specific heat and density can be taken using the physical mixture rule which gives a good agreement with the experimental works with an assumption of thermal equilibrium between the base fluid and nanoparticles [21].

$$C_{p,nf} = \frac{\varphi\rho_{np}C_{p,np} + (1-\varphi)\rho_{bf}C_{p,bf}}{\rho_{nf}} \tag{2}$$

The equation for density is given by:

$$\rho_{nf} = \varphi\rho_p + (1-\varphi)\rho_{bf} \tag{3}$$

2.2.2 Thermal conductivity

The thermal conductivity of Al_2O_3-water and CuO-water nanofluids can be calculated from the following correlation [22]. This correlation includes static part of Maxwell's theory and dynamic part which considers the Brownian motion of nanoparticles in the base fluid. Thermal conductivity of nanofluids depends on many factors like thermal conductivity, volume fraction, density, particle size of nanoparticle and thermal conductivity, density, specific heat capacity and temperature of the base fluid.

$$k_{effective} = k_{static} + k_{Brownian} \tag{4}$$

For spherical particles, the correlation for k_{static} is given by [23].

$$k_{static} = \frac{k_{np} + 2k_{bf} - 2(k_{bf} - k_{np})\varphi}{k_{np} + 2k_{bf} + (k_{bf} - k_{np})\varphi}k_{bf} \tag{5}$$

The term $k_{Brownian}$ is given by following correlation:

$$k_{Brownian} = 5\times10^4\beta\varphi\rho_{bf}C_{p,bf}\sqrt{\frac{\kappa T}{\rho_{np}d_{np}}}f(T,\varphi) \tag{6}$$

where correlation for $f(T,\varphi)$ is given by:

$$f(T,\varphi) = (2.8217\times10^{-2}\varphi + 3.917\times10^{-3})\frac{T}{T_0} + (-3.0669\times10^{-2}\varphi - 3.91123\times10^{-3})$$

β was estimated experimentally, For Al_2O_3-water nanofluids,

$\beta = 8.4407(100\varphi)^{-1.07304}$

For CuO-water nanofluids,

$\beta = 9.881(100\varphi)^{-0.9446}$

2.2.3 Viscosity

The viscosity of Al_2O_3-water and CuO-water nanofluid for different concentrations can be calculated from Einstein's equation [24] which is applicable to spherical particles, in volume fractions of less than 5.0% volume concentration and is defined as follows:

$$\mu_{nf} = \mu_{bf}(1 + 2.5\varphi) \tag{7}$$

2.3 Experimental setup

The schematic of the experimental setup is as shown in Fig. 2. It includes flow lines, a constant temperature bath, a centrifugal pump, flow meter, control valves, a flat tube radiator, a radiator fan, an air flow duct, a temperature controller, temperature sensors, a hot wire anemometer, temperature displays and pressure gauges. Nanofluids of different concentrations were prepared by using probe type sonicator. The prepared nanofluid was stored in a constant temperature bath with 15 *l* capacity. The temperature in the bath was maintained by using a heater and a temperature controller. The hot nanofluid was pumped using a centrifugal pump of 150 *W* capacity. A rotameter was used to measure the flow rate, with precision of ±0.1 *l/min* and the flow was controlled by a ball valve. The radiator used in this study was a cross-flow (single-pass) heat exchanger with the liquid-side unmixed and the air-side mixed. The photograph of radiator used in this study is shown in Fig. 4. The radiator was placed in an air flow duct which consists of 34 flat tubes and having a capacity of 0.8 *l*. Each tube was of 340 *mm* length, 17.6 *mm* width, 2.5 *mm* height and 0.45 *mm* thickness. Tubes and fins of the radiator were made of aluminium. The radiator was cooled using a fan with 120 W capacity. Air velocity was measured using a hot wire anemometer having ±0.1 *m/s* accuracy. Temperature of working fluid at the inlet and outlet of radiator was measured using RTD PT100 type sensor with an accuracy of ±0.1 °C. The surface temperature of the radiator tubes was measured using 6 K-type thermocouples with an accuracy of ±0.1 °C which were placed at different positions of radiator tube. Two bourdon pressure gauges were placed at the inlet and outlet of the radiator to measure the pressure drop of radiator. A 12 *V*, 40 A SMPS is used to convert 220 *V* AC to 12 *V* DC for the working of centrifugal pump and cooling fan. The photograph of the experimental setup is as shown in Fig. 3.

2.4 Equations used

The following procedure was used to obtain the heat transfer coefficient and Nusselt number.

According to Newton's law of cooling:

$$Q_{nf} = h_{in}A_{in}\Delta T = h_{in}A_{in}(T_{b,nf} - T_w) \tag{8}$$

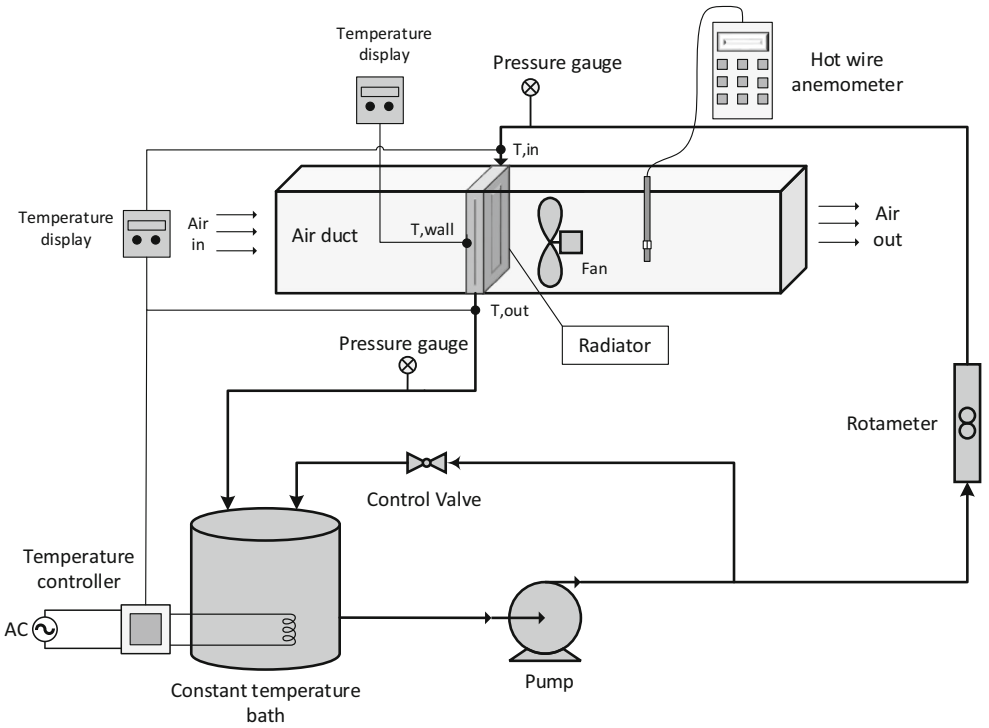


Fig. 2 Schematic diagram of experimental setup

where A_{in} is the inside surface area of the tube, h_{in} is the inside heat transfer coefficient and $T_{b,nf}$ is the bulk fluid temperature which is assumed to be the average of inlet and outlet temperature of fluid (Fig. 4).

$$T_{b,nf} = \frac{T_{nf,in} + T_{nf,out}}{2} \tag{9}$$

where $T_{nf,in}$ and $T_{nf,out}$ are the inlet and outlet temperatures respectively.

$$T_w = \frac{T_1 + T_2 + \ldots + T_6}{6} \tag{10}$$

where, T_w is the average surface temperature of the radiator tube wall and T_1 to T_6 denotes the temperature at different

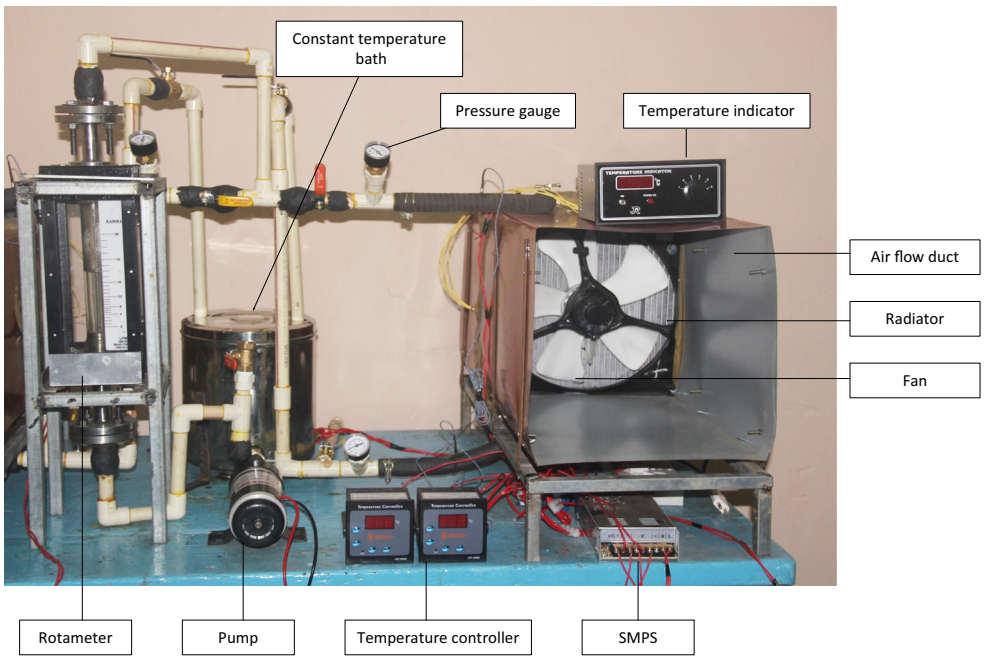


Fig. 3 Photograph of experimental setup



Fig. 4 Photograph of radiator

positions of radiator tube wall. In this study the resistance due to tube wall thickness was neglected since it is very small compared to convection resistance. Thus instead of measuring inside wall temperature, the outside wall temperature was measured assuming that there is no resistance due to wall thickness.

Heat transfer rate of nanofluid is given by:

$$Q_{nf} = \dot{m_{nf}} C_{p,nf} \Delta T = \dot{m_{nf}} C_{p,nf} (T_{nf,in} - T_{nf,out}) \quad (11)$$

where, $\dot{m_{nf}}$ is the mass flow rate and $C_{p,nf}$ is the specific heat of nanofluid.

Heat transfer rate of air is given by:

$$Q_a = \dot{m_a} C_{p,a} \Delta T = \dot{m_a} C_{p,a} (T_{a,in} - T_{a,out}) \quad (12)$$

where, $\dot{m_a}$ is the mass flow rate and $C_{p,a}$ is the specific heat of air. $T_{a,in}$ and $T_{a,out}$ are the inlet and outlet temperatures of air in the duct.

Tube side Nusselt number for experimental method is given by:

$$Nu_{exp} = \frac{h_{in,exp} d_{hyd}}{k_{nf}} \quad (13)$$

where, $h_{in,exp}$ is the inside heat transfer coefficient obtained from experimental method, d_{hyd} is the hydraulic mean diameter and k_{nf} is the thermal conductivity of nanofluid.

Tube side Nusselt number for numerical method is given by:

$$Nu_{num} = \frac{h_{in,num} d_{hyd}}{k_{nf}} \quad (14)$$

where, $h_{in,num}$ is the inside heat transfer coefficient obtained from experimental method.

Inside heat transfer coefficient from numerical method is given by:

$$h_{in,num} = \frac{\dot{q}}{(T_{wall} - T_b)} \quad (15)$$

where $\dot{q}$ is the heat flux at the wall, T_{wall} is the wall temperature and T_b is the bulk temperature of fluid. The values are taken from numerical simulation.

Outside heat transfer coefficient is given by:

$$h_o A_o = \frac{Q_a}{\Delta T} \quad (16)$$

where A_o is the outside surface area and h_o is the outside heat transfer coefficient, It is very difficult to measure the outside surface area due to complex fin arrangement. To overcome this a new term $h_{o,eff}$ was introduced which is called the effective heat transfer coefficient.

Effective heat transfer coefficient is given by

$$h_{o,eff} = \frac{h_o A_o}{A_{o,wf}} \quad (17)$$

where $A_{o,wf}$ is the outside surface area without fin. The effective heat transfer coefficient gives a value of outside heat transfer coefficient including the effect of fins.

Reynolds number of the nanofluid is given by:

$$Re_{nf} = \frac{\rho_{nf} V_{nf} d_{hyd}}{\mu_{nf}} \quad (18)$$

The performance of the heat exchangers is analyzed by the conventional ε-NTU technique and the effectiveness, ε is defined as:

$$\varepsilon = \frac{Q_{avg}}{(\dot{m} C_p)_{min} (T_{nf,in} - T_{a,in})} \quad (19)$$

where, Q_{avg} is the arithmetic average of heat transfer rate.

$$Q_{avg} = \frac{Q_{nf} + Q_a}{2} \quad (20)$$

The relation between effectiveness, ε and number of transfer units (NTU) is given by

$$\varepsilon = \frac{1}{C^*} \left[1 - e^{-C^* (1 - e^{NTU})} \right] \quad (21)$$

The capacity ratio C^* is given by:

$$C^* = \frac{(\dot{m} C_p)_{min}}{(\dot{m} C_p)_{max}} \quad (22)$$

The overall heat transfer coefficient can be calculated using the following equation:

$$NTU = \frac{UA}{(\dot{m} C_p)_{min}} \quad (23)$$

The inside overall heat transfer coefficient U_i can also be estimated from the following overall resistances.

$$\frac{1}{U_i A_i} = \frac{1}{h_o A_o} + \frac{\delta}{k_t A_t} + \frac{1}{h_i A_i} \quad (24)$$

where h is convection heat transfer coefficient, A_i is inside surface area, k_t is thermal conductivity of the tube wall, δ is the tube wall thickness, and the subscripts o, i, t denote air side, tube side and tube wall, respectively. The resistance

due to wall thickness was neglected in this study since its value is very small compared to convection resistance.

Colburn-Chilton factor is given by the equation:

$$j = \frac{h}{C_{p,nf}\rho_{nf}V_{nf}}\left(\frac{C_{p,nf}\mu_{nf}}{k_{nf}}\right)^{2/3} \tag{25}$$

The pressure drop in the radiator tube can be found by the following equation:

$$\Delta P = C_f \frac{4L}{d_{hyd}}\frac{1}{2}\rho V_{nf}^2 \tag{26}$$

where, C_f is the friction factor which can be obtained from computation, L is the length of the tube and V_{nf} is the velocity of nanofluid through the radiator tubes. The pumping power can be calculated from the pressure drop which is given by:

$$W = AV_{nf}(\Delta P) \tag{27}$$

where, ΔP is the pressure drop across the tube, A is the crossectional area of tube and V_{nf} is the velocity of nanofluid through the radiator tube.

2.5 Uncertainty analysis

The uncertainty analysis of calculated parameters such as Reynolds number, Nusselt number and heat transfer coefficient were estimated using uncertainties associated with individual measurements. Uncertainties of measured parameters such as flow meter, thermocouples, RTDs, Hot wire anemometer and pressure gauges were obtained from the manufacturer specifications. Kline-McClintok method [25] was used to calculate the uncertainties in the present study. According to this method, the function R is assumed to be calculated from a set of 'n' independent variables represented by;

$$R = R(x_1, x_2, x_3, ..., x_n) \tag{28}$$

Then the uncertainty w_R in the result can be determined by combining uncertainties of individual terms, given by the following equation;

$$w_R = \left[\left(\frac{\partial R}{\partial x_1}w_1\right)^2 + \left(\frac{\partial R}{\partial x_2}w_2\right)^2 + ... + \left(\frac{\partial R}{\partial x_n}w_n\right)^2\right]^{1/2} \tag{29}$$

where $w_1, w_2, ..., w_n$ are the uncertainties associated with the independent variables $x_1, x_2, ..., x_n$ respectively. From equation [29] the maximum uncertainties of Reynolds number, Nusselt number, effectiveness, inside heat transfer coefficient and outside heat transfer coefficient are ±3.34%, ±3.7%, ±3.94%, ±3.69% and ±2.81% respectively.

3 Numerical method

It is not feasible to conduct experiments for different concentrations and study the effect of nanofluids. Thus a simplified numerical model of the flat tube radiator was studied. The numerical model considers only a single tube of the flat tube radiator. The effect of fins and tube thickness were taken into consideration by providing proper boundary conditions, which were calculated from conducting experiments. The numerical study was carried out in Ansys Fluent (2015).

3.1 Problem geometry

A single flat tube of the radiator was used for numerical study. The dimensions of the numerical model was the same as that of the radiator used in the experiment. The radiator tube is of 340 *mm* length, 17.6 *mm* width, 2.5 *mm* height and 0.45 *mm* thickness. Geometry of the flat tube is as shown in Fig. 5

3.2 Governing equations

The working fluid used in the radiator can be taken as incompressible and Newtonian fluid. The effect of viscous dissipation and radiative effect are not considered. Due to very low particle size and concentration of nanoparticles in the base fluid, the nanofluid is assumed to be a single phase fluid [12]. Under these assumptions the flow and heat transfer were solved in three dimensional cartesian coordinates. The following conservation equations were solved in Ansys Fluent (2015).

3.2.1 Continuity equations

The continuity equation solved in three dimensional Cartesian coordinate system is given as:

$$(\nabla . V) = 0 \tag{30}$$

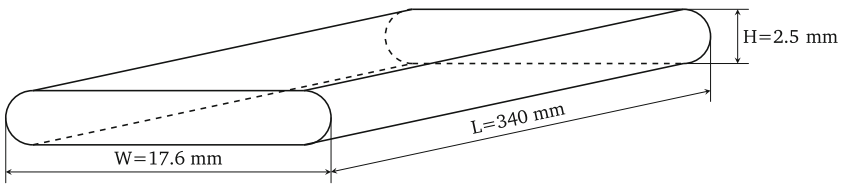


Fig. 5 Geometry and dimensions of flat tube



Fig. 6 Crossectional view of mesh

3.2.2 Momentum equations

The momentum equation solved in three dimensional Cartesian coordinate system is given as:

$$\rho(\nabla.V)V = -\nabla P + \mu\nabla^2 V \tag{31}$$

3.2.3 Energy equations

The energy equation solved for calculation of temperature distribution is given as:

$$\rho C_p(\nabla.V)T = \nabla^2(kT) \tag{32}$$

3.3 Boundary conditions

The continuity, momentum and energy equations were solved subjected to the following boundary conditions. At the inlet of flat tube, uniform axial velocity and constant temperature were given (u = v = 0, w = w_∞). The inlet velocity was varied according to different Reynolds numbers. The temperature at the inlet was given as 363 K corresponding to the temperature of coolant from the engine block. At the outlet of the flat tube, pressure outlet boundary condition was adopted with zero gauge pressure (P = P_{atm}). No slip boundary condition was provided at the wall of radiator tube for velocity (u = v = w = 0). For the radiator realistic thermal boundary condition, the outside wall is prescribed as convective heat transfer coefficient h_o on the air side and a fixed free stream temperature ($-k\frac{\partial T}{\partial x} = h_o[T_\infty - T_w]$). The outside heat transfer coefficient were calculated from experiments. The effective outside heat transfer coefficient which compensate for the effect of fins in the actual radiator was given as the convective heat transfer boundary condition in the tube wall. The average value of effective heat transfer coefficient was taken as 350 W/m^2K. Experimentally measured ambient temperature was provided at the wall boundary.

3.4 Numerical computation

The system of governing equations [30–32] coupled with the above boundary conditions were solved by control volume approach in Ansys Fluent 15. A staggered grid scheme was used, in which the velocity components were evaluated at the control volume faces, while the rest of the variables governing the flow field were stored at the central node of the control volume. Pressure-Velocity coupling were done using semi implicit (SIMPLE) method. Least square cell based interpolation method was used for calculating cell-face pressures in order to compute pressure gradient. A second-order scheme was employed to discretize the pressure terms and second-order upwind scheme was employed to discretize momentum terms and energy terms. The convergence criteria for all simulations performed in this work were considered when the residuals of continuity, momentum and energy terms are lower than 10^{-6}. From the post processing of the numerical simulation, the values of bulk temperature, average wall temperature, average wall heat flux, convective heat transfer coefficient and skin friction factor were calculated.

3.5 Grid independence study

A three dimensional mesh was generated using ICEM CFD. Crossectional view of the mesh is shown in Fig. 6. In order to confirm that the results of numerical computation is independent of grid size, grid independence study was done. Four different meshes were generated. Mesh-1(72×14×112), Mesh-2(100×21×150), Mesh-3(125×75×200) and Mesh-4(150×75×225). Computations were carried out for all the four meshes with same boundary conditions. Results of average temperature and average velocity at Z = 0.15 m and X = 0 were compared. The converged solutions of 4 different meshes are listed in Table 2. Results of mesh-1, mesh-2, and mesh-3 shows some variation, but the results of mesh-3 and mesh-4 overlaps. Therefore it can be concluded that mesh-3 is the most effective mesh because there is no variation in results even after increasing the grid density. Thus mesh-3 was selected and used throughout this study.

Table 2 Average temperature and average velocity at Z = 0.15 m and X = 0 for four different meshes

Grid	Velocity [m/s]	Temperature [K]
Mesh-1(72 ×14×112)	0.049667	351.948
Mesh-2(100×21×150)	0.049830	351.956
Mesh-3(125×75×200)	**0.050011**	**351.964**
Mesh-4(150×75×225)	0.050014	351.965

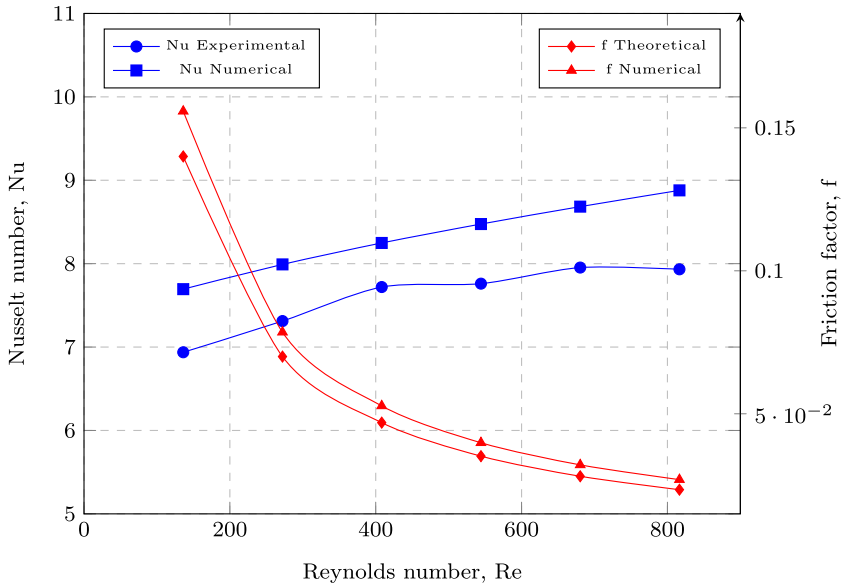


Fig. 7 Comparison of experimental and numerical results of 0.05% volume concentration of CuO-water nanofluid

3.6 Validation of numerical method

Numerical results were validated by comparing with experimental results and theoretical correlations. Experimental results were obtained from conducting experiments in flat tube radiator. The working fluid recirculates through the radiator with constant inlet temperature of 90 °C. Experiments were conducted by varying the Reynolds numbers from 136 to 816 for water, 0.05% volume concentration of Al_2O_3-water nanofluid and 0.05% volume concentration of CuO-water nanofluid. The numerical values of Nusselt number and friction factor for different Reynolds numbers of nanofluids were compared with the experimental results and theoretical correlations. The comparison between experiment and numerical results of CuO-water and Al_2O_3-water nanofluids are shown in Figs. 7 and 8 respectively. For six different Reynolds numbers, the maximum deviation in Nusselt number and friction factor are 10.1% and 9.8% respectively. The difference in experimental and numerical results are due to uncertainties in experimental measurements and assumptions regarding neglecting the tube thickness resistance. Also the axial conduction through the tube wall is not considered in numerical method.

4 Results and discussions

4.1 Thermal conductivity enhancement

Figure 9 shows the variation of thermal conductivity of CuO-water and Al_2O_3-water nanofluids for different concentrations. It is observed that the thermal conductivity

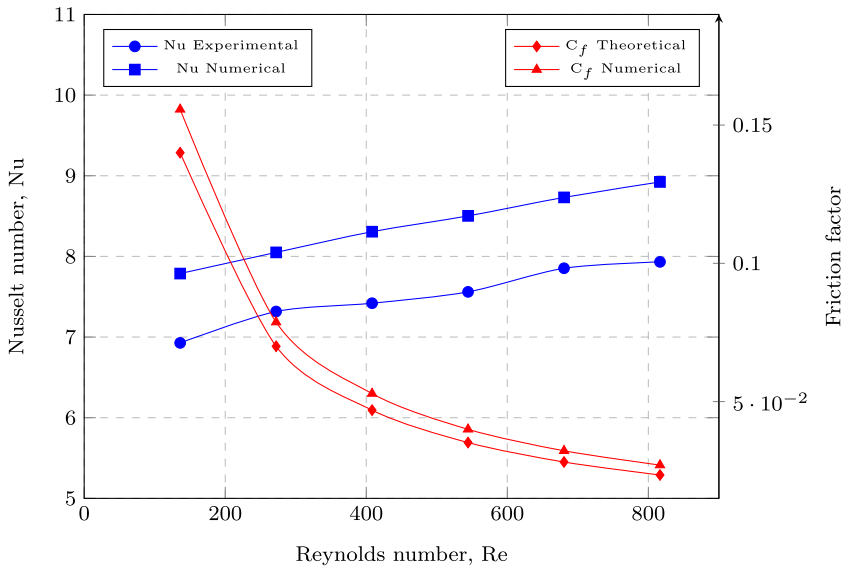


Fig. 8 Comparison of experimental and numerical results of 0.05% volume concentration of Al_2O_3-water nanofluid

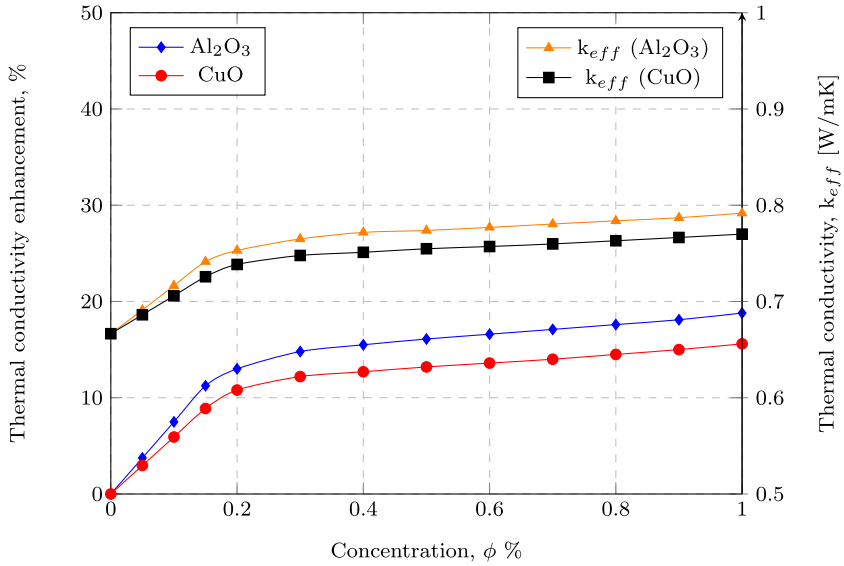


Fig. 9 Thermal conductivity of nanofluids and enhancement in thermal conductivity of nanofluids compared to water for different concentrations

of both nanofluids increases with increasing concentration. The enhancement is more for Al_2O_3-water nanofluid compared to CuO-water nanofluid. The results shows that for 1% volume concentration, the thermal conductivity increased by 19.11% and 15.66% for Al_2O_3-water and CuO-water nanofluids respectively. Even though the thermal conductivity of CuO is more compared to Al_2O_3 nanoparticles, due to higher density of CuO nanoparticle, the effect of Brownian motion is less. Thus Al_2O_3 nanofluids are more preferred due to its higher effective thermal conductivity and lower density, which also reduces the sedimentation.

4.2 Experimental results

4.2.1 Variation of Nusselt number

Figure 10 shows the variation of Nusselt number with Reynolds number from experimental results. The results are obtained from conducting experiments for water, 0.05% volume concentrations of Al_2O_3-water and CuO-water nanofluids. It is observed that Nusselt number increases with increase in Reynolds number. For both nanofluids, with the addition of nanoparticles the number decreases compared to water. This is because, although the heat transfer

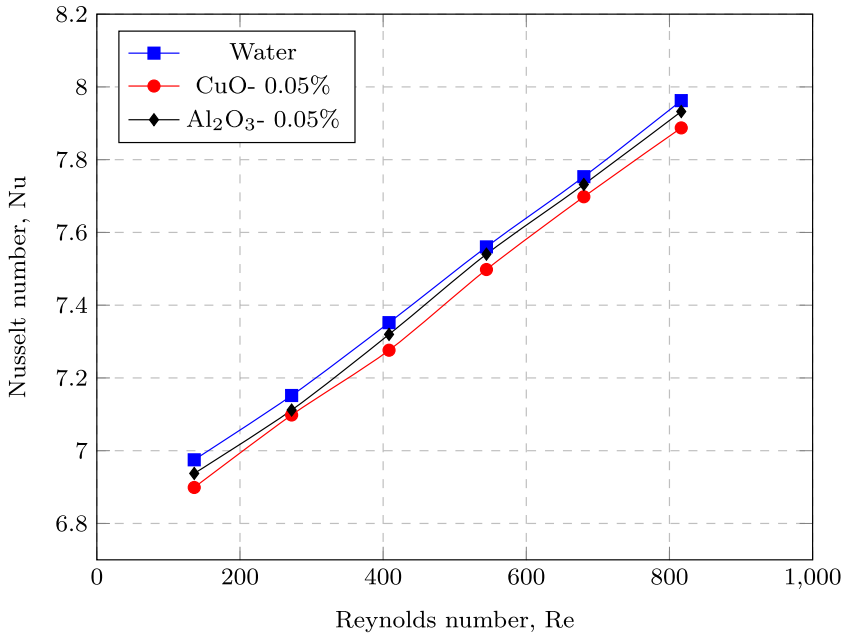


Fig. 10 Variation of Nusselt number with Reynolds number for water and 0.05% volume concentrations of CuO and Al_2O_3 nanofluids

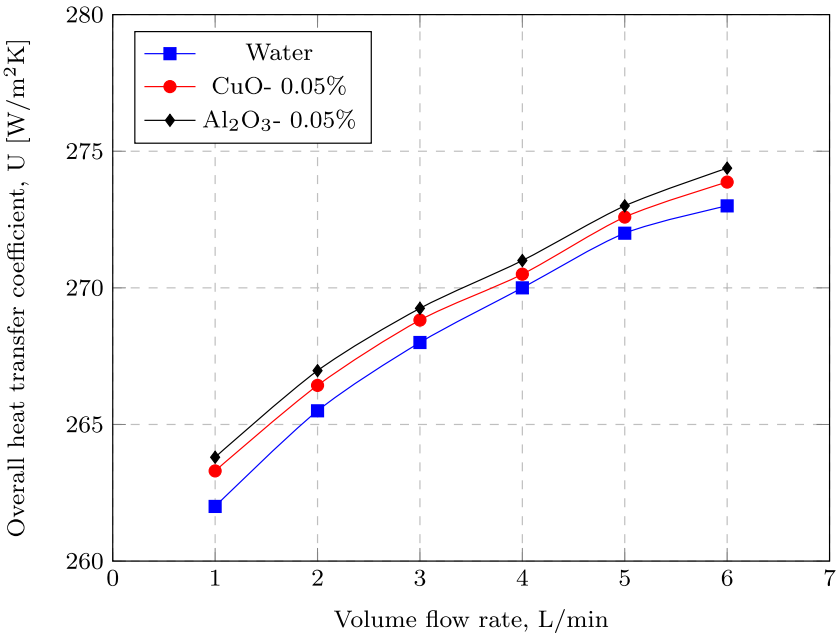


Fig. 11 Variation of overall heat transfer coefficient with flow rate for water and 0.05% volume concentrations of CuO and Al_2O_3 nanofluids

coefficient increases with increase in concentration, the increase in the heat transfer coefficient is less when compared to the increase in thermal conductivity. Al_2O_3-water nanofluid is found to be having higher enhancement compared to CuO-water nanofluid due to its higher effective thermal conductivity.

4.2.2 Variation of overall heat transfer coefficient

Figure 11 shows the variation of overall heat transfer coefficient with the flow rate from experimental results. The results are obtained from conducting experiments for water, 0.05% volume concentrations of Al_2O_3-water and CuO-water nanofluids. It is observed that the overall heat transfer coefficient increases with increase in flow rate. For both nanofluids, as the concentration increases the heat transfer coefficient also increases. Maximum enhancement of 0.5% and 0.38% are obtained for Al_2O_3-water and CuO-water nanofluids respectively. Al_2O_3-water nanofluid is found to be having higher enhancement compared to CuO-water nanofluid due to its higher effective thermal conductivity.

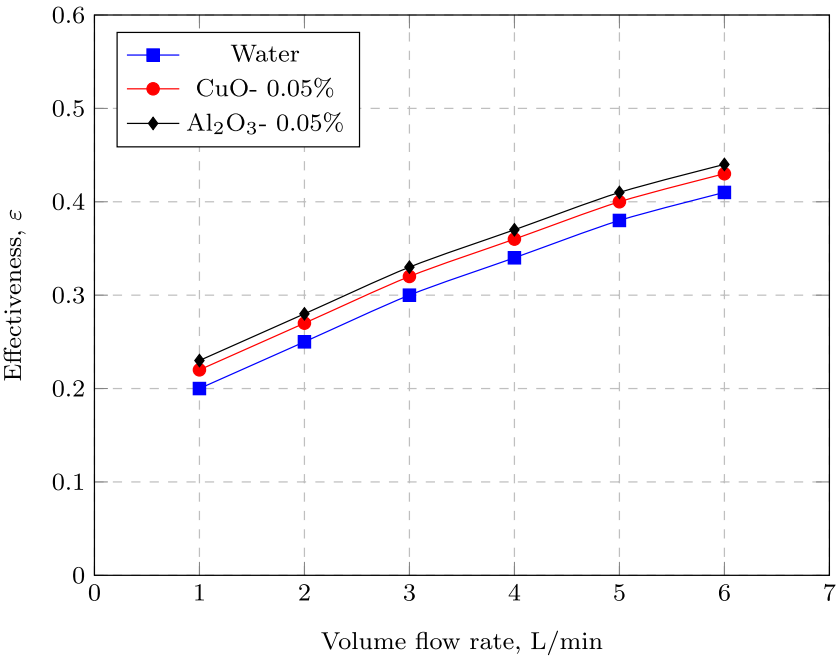


Fig. 12 Variation of effectiveness of radiator with flow rate for water and 0.05% volume concentrations of CuO and Al_2O_3 nanofluids

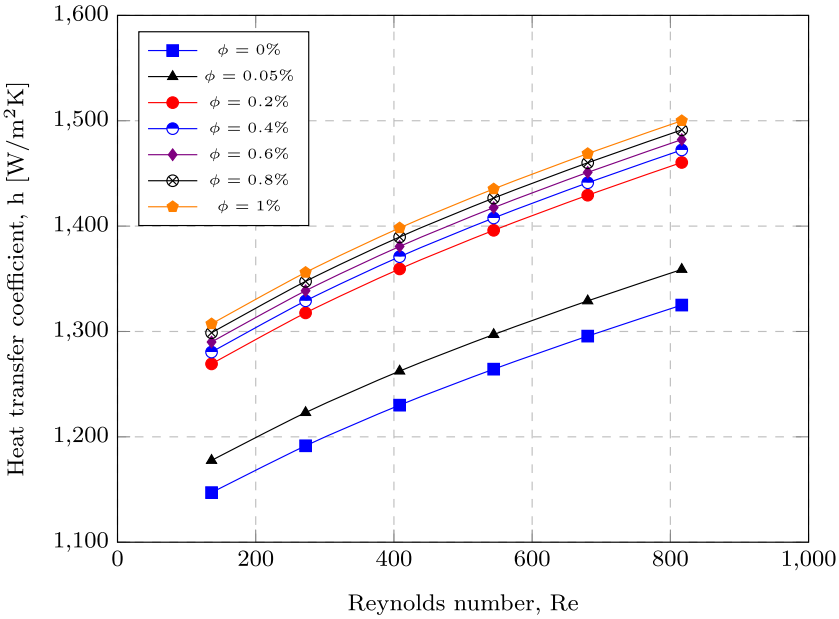


Fig. 13 Variation of inside heat transfer coefficient with Reynolds number for different concentrations of CuO-water nanofluid

4.2.3 Variation of effectiveness

Figure 12 shows the variation of effectiveness of radiator with the flow rate from experimental results. The results are obtained from conducting experiments for water, 0.05% volume concentrations of Al_2O_3-water and CuO-water nanofluids. It is observed that the effectiveness of radiator increases with increasing flow rate. The effectiveness of radiator also increases when nanoparticles are added, due to the increase in heat rejection. Maximum enhancement of 7.3% and 4.8% are obtained for Al_2O_3-water and CuO-water nanofluids respectively. Al_2O_3-water nanofluid is found to be having higher enhancement compared to CuO-water nanofluid due to its higher effective thermal conductivity.

4.3 Numerical results

4.3.1 Variation of inside heat transfer coefficient

Figures 13 and 14 shows the variation of inside heat transfer coefficient with Reynolds number for different concentrations of CuO-water and Al_2O_3-water nanofluids respectively. It is observed that the heat transfer coefficient increases with increase in Reynolds number and with increase in concentration. In the case of 1% concentration

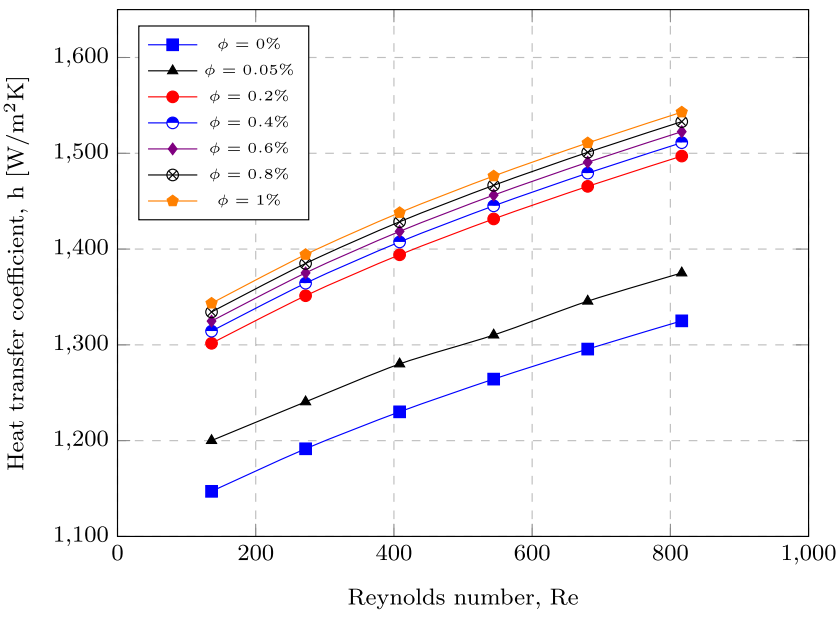


Fig. 14 Variation of inside heat transfer coefficient with Reynolds number for different concentrations of Al_2O_3-water nanofluid

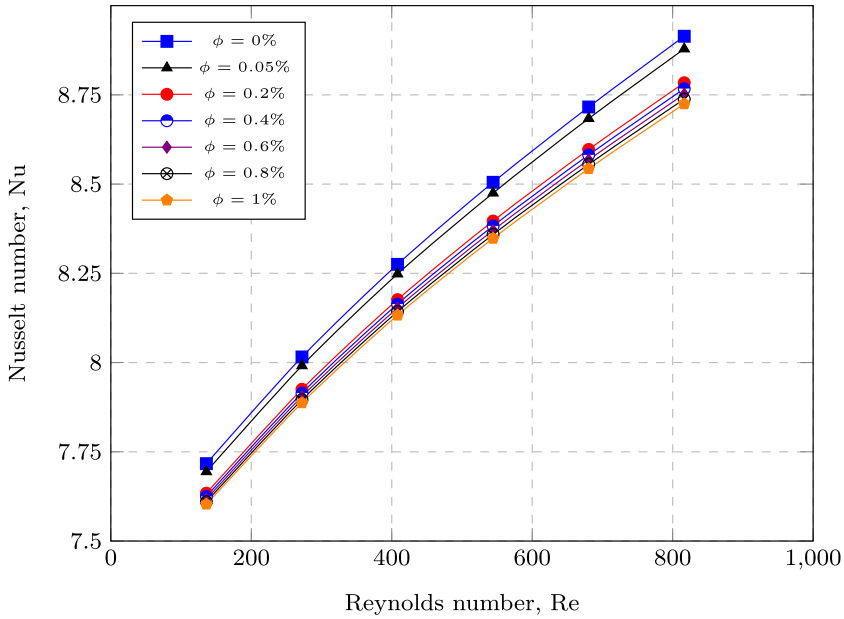


Fig. 15 Variation of Nusselt number with Reynolds number for different concentrations of CuO-water nanofluid

of CuO-water and Al_2O_3-water nanofluids, the maximum heat transfer coefficient enhancement of 13.2% and 16.4% are obtained respectively compared to the base fluid for Reynolds number 816. The increase in heat transfer coefficient is due to the increase in thermal conductivity of nanofluid when nanoparticles were dispersed. The increase in effective thermal conductivity leads to the increase in heat transfer coefficient. The results shows same trend as that of experimental results. Compared to CuO-water nanofluids, Al_2O_3-water nanofluids gives maximum enhancement in heat transfer coefficient due to its higher effective thermal conductivity.

4.3.2 Variation of Nusselt number

Figures 15 and 16 shows the variation of Nusselt number with Reynolds number for different concentrations of CuO-water nanofluid and Al_2O_3-water nanofluid respectively. The Nusselt number increases with increase in Reynolds number. With an increase in the concentration, the Nusselt number decreases. This is because, although the heat transfer coefficient increases with increase in concentration, the increase in the heat transfer coefficient is less when compared to the increase in thermal conductivity. As an example, the percentage increase in the thermal conductivity of

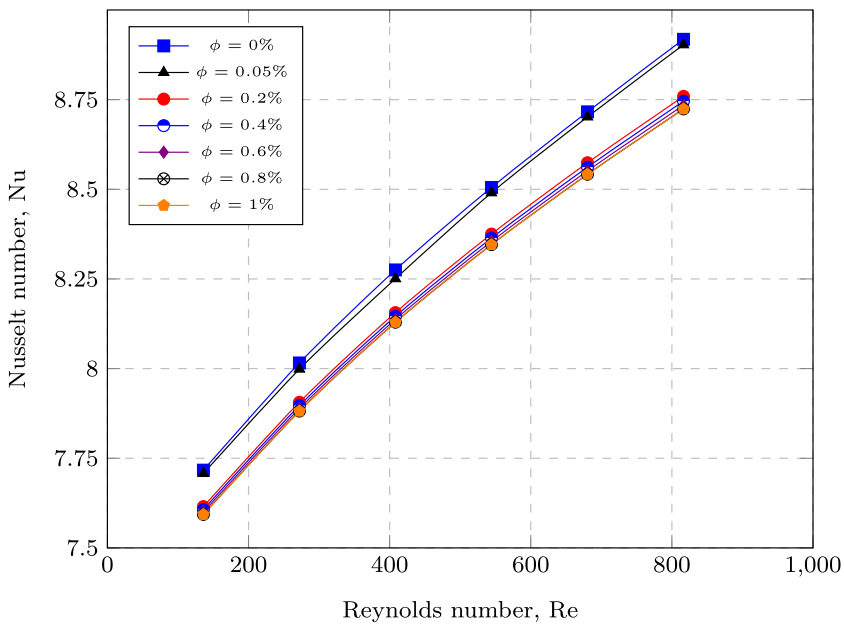


Fig. 16 Variation of Nusselt number with Reynolds number for different concentrations of Al_2O_3-water nanofluid

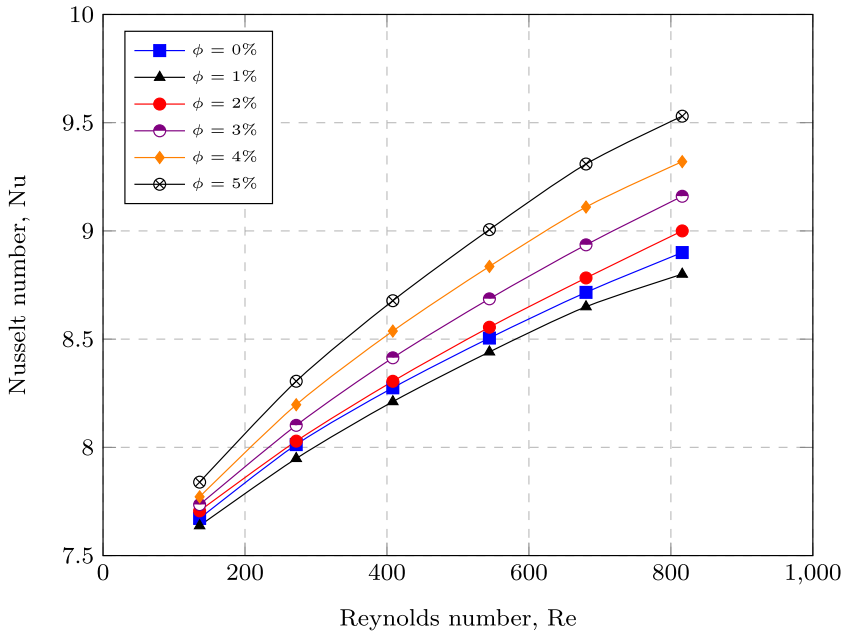


Fig. 17 Variation of Nusselt number with Reynolds number for higher concentrations of CuO-water nanofluid

1% concentration of CuO-water nanofluid over the base fluid is 15.66%. For the same concentration, we observe from Fig. 13 that there is an increase in the heat transfer coefficient of 13.2% over the base fluid for a Reynolds number of 816. The trend is same for Al_2O_3-water nanofluid also.

4.3.3 Variation of Nusselt for higher concentrations

Figures 17 and 18 shows the variation of Nusselt number with Reynolds number for higher concentrations of CuO-water nanofluid and Al_2O_3-water nanofluid respectively. Nusselt number was calculated for higher concentrations of nanofluids upto 5%. It is observed from Fig. 15 that for CuO-water nanofluid the Nusselt number decreases with increasing concentration upto 1%. But when the concentration increases beyond 1%, the Nusselt number increases. This is because, increasing concentration beyond 1%, the increase in heat transfer coefficient is more compared to increase in thermal conductivity. The maximum increase in Nusselt number of 7% is obtained in 5% concentration of CuO-water nanofluid for Re = 816. Similarly for Al_2O_3-water nanofluid also the Nusselt number decreases with increasing concentration upto 1% and increases by further

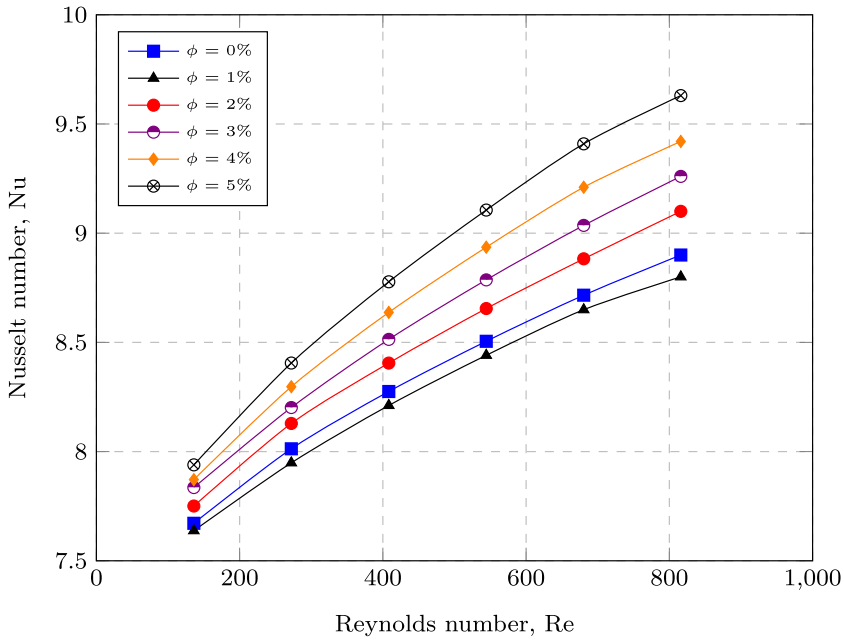


Fig. 18 Variation of Nusselt number with Reynolds number for higher concentrations of Al_2O_3-water nanofluid

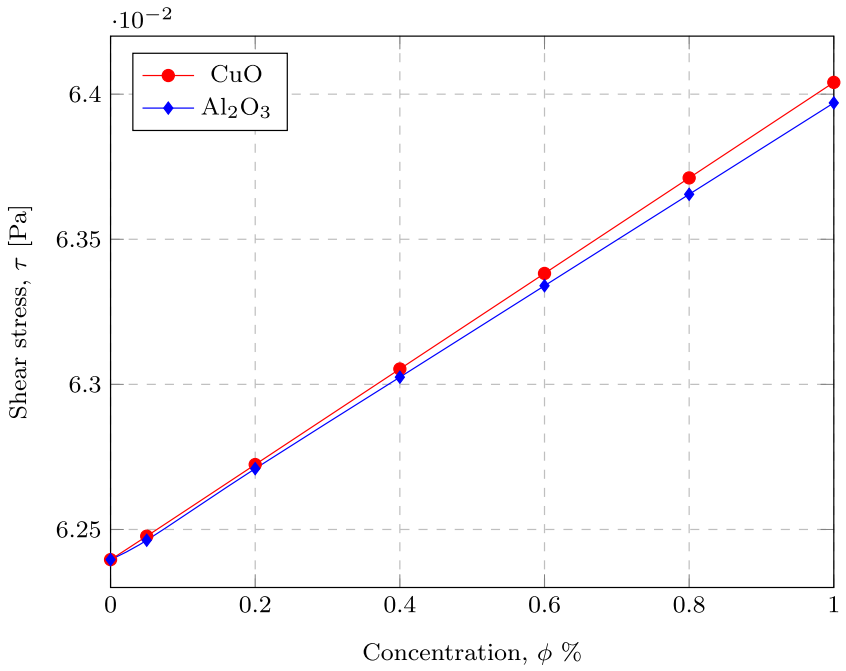


Fig. 19 Variation of shear stress with increase in concentration for same inlet velocity

increasing concentration. The maximum increase in Nusselt number of 8.2% is obtained in 5% concentration of Al_2O_3-water nanofluid for Re = 816.

4.3.4 Variation of shear stress

Figure 19 shows the variation of average shear stress on the tube wall for different volume concentrations of Al_2O_3-water and CuO-water nanofluids. The results shows an increase in average shear stress on the tube wall with increasing concentration. Compared to the base fluid, the shear stress is increased by 2.52% and 2.63% for Al_2O_3-water and CuO-water nanofluids respectively for 1% volume concentration. The increase in shear stress is due to the increase in viscosity of nanofluids when concentration increases. Thus increasing the volume concentration will increase the shear stress, which is a disadvantage for nanofluids.

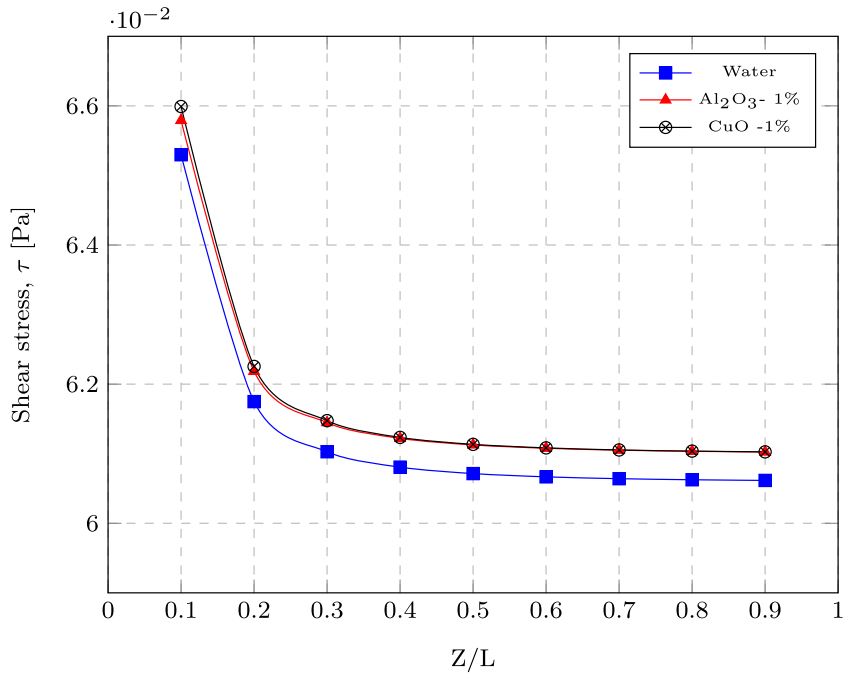


Fig. 20 Variation of shear stress along the tube length for water and 1% volume concentration of Al_2O_3-water and CuO-water nanofluids

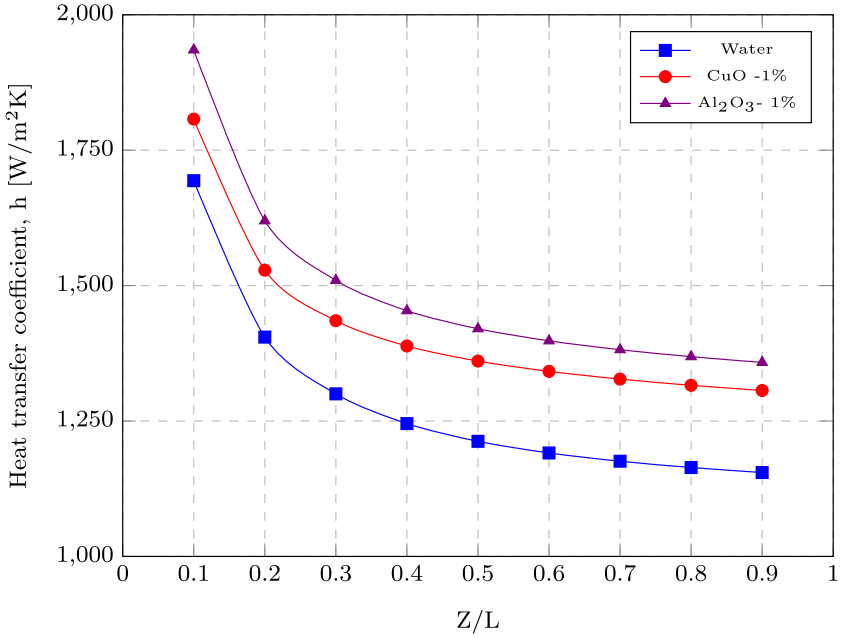


Fig. 21 Variation of Heat transfer coefficient along the tube length for Re = 816

4.3.5 Variation of shear stress along tube length

Figure 20 shows the variation of shear stress along the tube length for water and 1% volume concentration of Al_2O_3-water and CuO-water nanofluids. It is observed that shear stress decreases in developing flow region and remains constant after the flow is fully developed. The hydrodynamic entry length of the flow can be calculated from the equation, $X_H = 0.05 \mathrm{ReD}_{hyd}$. From the above equation and Fig. 20 it is found that the flow is is developing upto Z/L = 0.52 and becomes fully developed after that. In addition to that as the concentration of nanofluid increases the shear stress also increases. This is due to the increase in viscosity of the nanofluid in addition of nanoparticles.

4.3.6 Variation of heat transfer coefficient along tube length

Figure 21 shows the variation of heat transfer coefficient along the tube length for water and 1% volume concentration of Al_2O_3-water and CuO-water nanofluids. The thermal entry length of the flow can be calculated from the equation, $X_H = .05 \mathrm{RePrD}_{hyd}$. From the above equation and Fig. 21 it is found that the flow is thermally developing flow. In

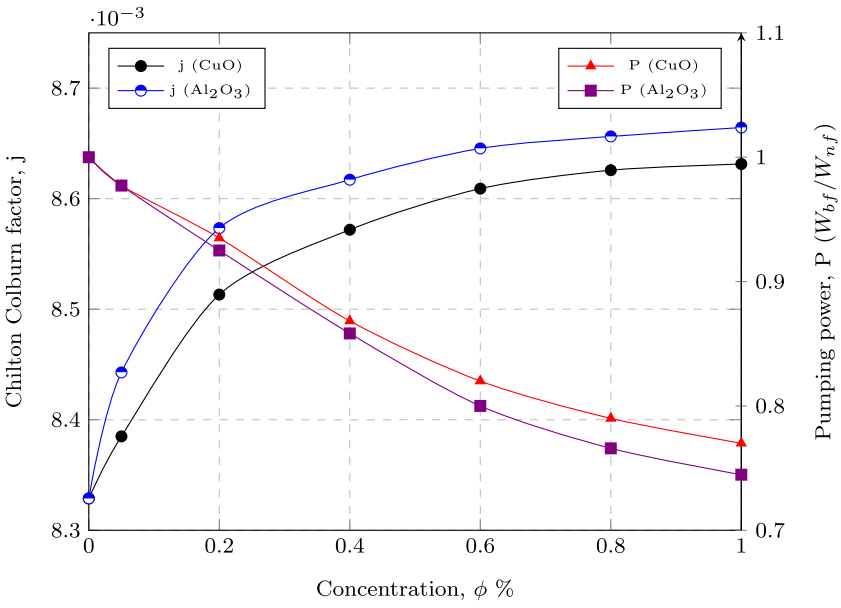


Fig. 22 Variation of Chilton-Colburn factor and pumping power factor for different volume concentrations of CuO and Al_2O_3 nanofluids

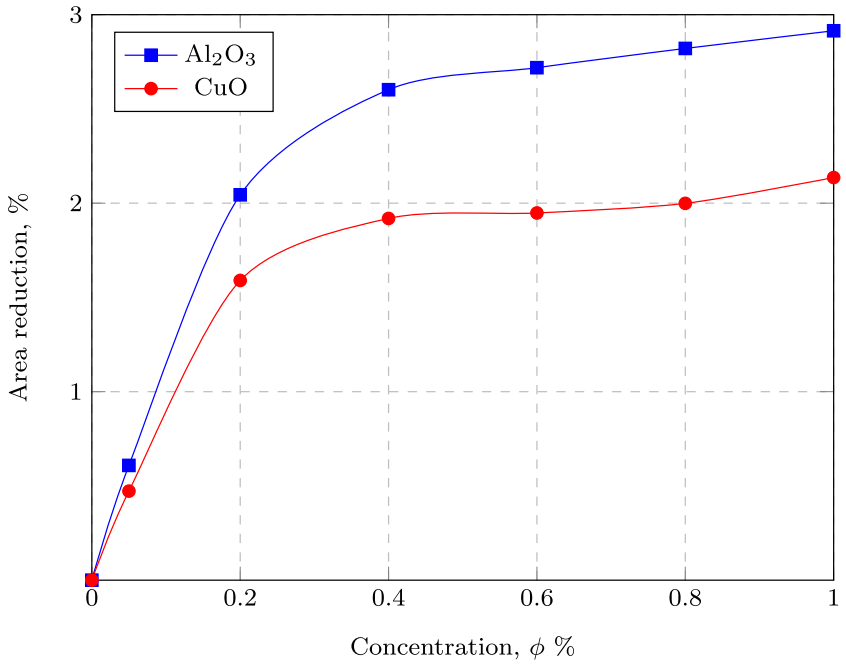


Fig. 23 Reduction in surface area of radiator for same heat rejection

addition to that as the concentration of nanofluid increases, the heat transfer coefficient also increases. This is due to the increase in thermal conductivity of the nanofluid in addition of nanoparticles. The enhancement in heat transfer coefficient is more for Al_2O_3-water nanofluids due to its higher thermal conductivity.

4.3.7 Variation of Chilton-Colburn factor and pumping power

Figure 22 shows the variation of Chilton-Colburn factor and pumping power for different concentrations of Al_2O_3-water and CuO-water nanofluids. With an increase in the concentration, the Chilton-Colburn factor increases. This is because the heat transfer enhancement is more predominant than frictional losses. As the concentration increases, although an increase in heat transfer coefficient is obtained, the frictional losses due to increase in viscosity of nanofluid is also increasing. As the concentration increases upto 0.4% volume concentration, the slope of the graph decreases and there is no much increase after reaching 0.8% volume concentration. Figure 22 also illustrates the pumping power variation for different concentrations. For the same heat rejection from water at Re = 816, the corresponding pumping power for different concentrations were plotted. The results shows that the pumping power decreases as the concentration decreases. There is no much reduction in pumping power by increasing concentration more than 0.8% volume concentration. The pumping power reduced by 0.74 times and 0.77 times for Al_2O_3-water and CuO-water nanofluids respectively for 1% volume concentration. By comparing both enhancement in heat transfer and increase in frictional losses, 0.4% to 0.8% volume concentration gives the optimum concentration in which heat transfer enhancement factor is more predominant. This study has not been reported in literature.

4.3.8 Area reduction

Figure 23 shows the surface area reduction of flat tube radiator when nanofluids are used as a coolant instead of conventional coolants. It is observed that as the concentration increases the surface area of radiator can be reduced. For the same heat rejection of water, the surface area can be reduced by 2.1% for CuO-water nanofluid and 2.9% for Al_2O_3-water nanofluid. There is no much reduction in surface area by increasing concentration more than 0.8% volume concentration.

5 Conclusions

The convective heat transfer in laminar flow inside a flattened tube of an automobile radiator using Al_2O_3-water and CuO-water nanofluids were investigated experimentally and numerically. Nanofluids of 0.05% volume concentrations were prepared with Al_2O_3 and CuO nanoparticles. The numerical results were validated by using experimental results of both nanofluids. The experiments were conducted for water and 0.05% volume concentrations of Al_2O_3-water and CuO-water nanofluids by varying the Reynolds numbers from 136 to 816 (1-6 *l/min*).

- The experimental study shows an enhancement in overall heat transfer coefficient by the addition of nanoparticles in the base fluid. Maximum enhancement of 0.5% and 0.38% obtained for 0.05% concentration of Al_2O_3-water and CuO-water nanofluids respectively. The experimental results shows that the effectiveness of radiator increases with increasing flow rate and concentration. An effectiveness of 0.44 is obtained for 0.05% volume concentration of Al_2O_3 nanofluid at 6 l/min, and which is 7.3% more than that of water at same flow rate.
- The numerical works were extended for various number of concentrations. The numerical analysis shows a substantial enhancement in heat transfer coefficient by the addition of nanoparticles in the base fluid. A maximum enhancement of 13.2% and 16.4% in heat transfer coefficient were obtained for 1% concentration of CuO and Al_2O_3 nanofluids respectively for $Re = 816$.
- The Nusselt number increases with the increase in Reynolds number. The maximum increase in Nusselt number of 7% and 8.2% were obtained in 5% concentration of CuO and Al_2O_3 nanofluids respectively for $Re = 816$.
- Chilton Colburn factor (j) increases with increase in concentration for both nanofluids. For 1% concentration j, increased by 3.6% and 4% for CuO and Al_2O_3 nanofluids respectively. The increase in Chilton-Colburn factor shows that the heat transfer enhancement factor is more predominant than the frictional loss factor.
- For same heat rejection of water, the pumping power was reduced by 0.74 times for 1% of CuO and 0.77 times for 1% of Al_2O_3 nanofluids. The surface area of radiator can be reduced by using nanofluids instead of conventional coolants. For same heat rejection of water, the area of the radiator can be reduced by 2.1% and 2.9% for 1% concentration of CuO and Al_2O_3 nanofluids respectively.

The variation of Chilton-Colburn factor, pumping power and area reduction factor shows that the advantage of increasing concentration is less above 0.8% volume concentration. Thus the concentration between 0.4% to 0.8% can be taken as the optimum concentration for nanofluids. Al_2O_3-water nanofluids are more preferred than CuO-water nanofluids due to the higher effective thermal conductivity of Al_2O_3 nanofluids compare to CuO nanofluids. By considering all the above factors, heat rejection from engines can be enhanced by using nanofluids with optimum concentration, in automobile radiator instead of conventional coolants like water/ethylene glycol.

Acknowledgments The authors gratefully acknowledge Centre for Engineering Research and Development(CERD) for providing financial support for the present research work (KTU/CERD/387/2015).

References

1. Zhu HT, Lin YS, Yin YS (2004) A novel one-step chemical method for preparation of copper nanofluids. J Colloid Interface Sci 277(1):100–103
2. Nguyen CT, Desgranges F, Roy G, Galanis N, Maré T, Boucher S, Angue Mintsa H (2007) Temperature and particle-size dependent viscosity data for water-based nanofluids – hysteresis phenomenon. Int J Heat Fluid Flow 28(6):1492–1506. Revised and extended papers from the 5th conference in Turbulence, Heat and Mass Transfer'The 5th conference in Turbulence, Heat and Mass Transfer
3. Hwang Y, Lee J-K, Lee J-K, Jeong Y-M, Cheong SI, Ahn Y-C, Kim SH (2008) Production and dispersion stability of nanoparticles in nanofluids. Powder Technol 186(2):145–153
4. Choi C, Yoo HS, Oh JM (2008) Preparation and heat transfer properties of nanoparticle-in-transformer oil dispersions as advanced energy-efficient coolants. Curr Appl Phys 8(6):710–712. Nano Korea 2006 Symposium 4th Nano Korea 2006 Symposium
5. Zhu H, Han D, Meng Z, Daxiong W, Zhang C (2011) Preparation and thermal conductivity of cuo nanofluid via a wet chemical method. Nanoscale Res Lett 6(1):1–6
6. Wei Y, Xie H (2012) A review on nanofluids Preparation, stability mechanisms, and applications. J Nanomaterials 2012:1:1–1:17
7. Chang M-H, Liu H-S, Tai CY (2011) Preparation of copper oxide nanoparticles and its application in nanofluid. Powder Technol 207(1–3):378–386
8. Jang SP, Choi SUS (2004) Role of brownian motion in the enhanced thermal conductivity of nanofluids. Appl Phys Lett, 84(21)
9. Yu W, Choi SUS (2003) The role of interfacial layers in the enhanced thermal conductivity of nanofluids: a renovated maxwell model. J Nanoparticle Res 5(1):167–171
10. Vajjha RS, Das DK (2009) Experimental determination of thermal conductivity of three nanofluids and development of new correlations. Int J Heat Mass Transf 52(21–22):4675–4682
11. Bigdeli MB, Fasano M, Cardellini A, Chiavazzo E, Asinari P (2016) A review on the heat and mass transfer phenomena in nanofluid coolants with special focus on automotive applications. Renew Sust Energ Rev 60:1615–1633
12. Kakaç S, Pramuanjaroenkij A (2016) Analysis of convective heat transfer enhancement by nanofluids single-phase and two-phase treatments. J Eng Phys Thermophys 89(3):758–793
13. Bozorgan N, Krishnakumar K, Bozorgan N (2012) Numerical study on application of cuo-water nanofluid in automotive diesel engine radiator. Modern mechanical engineering 2(04):130
14. Chiam HW, Azmi WH, Usri NA, Mamat R, Adam NM (2017) Thermal conductivity and viscosity of al 2 o 3 nanofluids for different based ratio of water and ethylene glycol mixture. Exp Thermal Fluid Sci 81:420–429
15. Bayat J, Nikseresht AH (2011) Investigation of the different base fluid effects on the nanofluids heat transfer and pressure drop. Heat mass transf 47(9):1089–1099
16. Sahoo RR, Sarkar J (2016) Heat transfer performance characteristics of hybrid nanofluids as coolant in louvered fin automotive radiator. Heat Mass Transf, 1–9
17. Vajjha RS, Das DK, Namburu PK (2010) Numerical study of fluid dynamic and heat transfer performance of al_2o_3 and cuo nanofluids in the flat tubes of a radiator. Int J Heat Fluid Flow 31(4):613–621
18. Peyghambarzadeh SM, Hashemabadi SH, Seifi Jamnani M, Hoseini SM (2011) Improving the cooling performance of automobile radiator with al_2o_3/water nanofluid. Appl Therm Eng 31(10):1833–1838
19. Peyghambarzadeh SM, Hashemabadi SH, Hoseini SM, Seifi Jamnani M (2011) Experimental study of heat transfer enhancement

using water/ethylene glycol based nanofluids as a new coolant for car radiators. Int Commun Heat Mass Transf 38(9):1283–1290
20. Durga Prasad PV, Gupta AVSSKS, Sreeramulu M, Syam Sundar L, Singh MK, Sousa ACM (2015) Experimental study of heat transfer and friction factor of al_2o_3 nanofluid in u-tube heat exchanger with helical tape inserts. Exp Thermal Fluid Sci 62:141–150
21. Xuan Y, Roetzel W (2000) Conceptions for heat transfer correlation of nanofluids. Int J Heat Mass Transf 43(19):3701–3707
22. Ray DR, Das DK, Vajjha RS (2014) Experimental and numerical investigations of nanofluids performance in a compact minichannel plate heat exchanger. Int J Heat Mass Transf 71:732–746
23. Maxwell JC (1873) A treatise on electricity and magnetism, vol 1, 1st edn. Clarendon press, Oxford
24. Einstein A (1956) Investigations on the theory of the Brownian movement courier corporation
25. Kline SJ, McClintock FA (1953) Describing uncertainties in single-sample experiments. Mech Eng 75(1):3–8